

https://doi.org/10.1070/QEL16902

Monitoring of chlorin-based photosensitiser localisation with dual-wavelength fluorescence imaging: numerical simulations

A.V. Khilov, D.A. Kurakina, I.V. Turchin, M.Yu. Kirillin

Abstract. **An approach to the estimation of chlorin-based photosensitiser localisation with dual-wavelength fluorescence imaging after topical application or intravenous injection is developed based on numerical simulations. Fluorescence imaging, which is commonly used for the monitoring of photosensitiser distribution within tissue, does not allow for its depth-resolved imaging. Chlorin-based photosensitisers feature two peaks in their absorption spectra corresponding to 402 and 662 nm, which allows for fluorescence excitation at two wavelengths with significantly different light penetration depths into biotissues. The ratio of fluorescence signals detected upon irradiation at different excitation wavelengths is shown to provide the information about photosensitiser localisation. The cases of exponential in-depth decay of the photosensitiser concentration and uniform photosensitiser distribution within the layer at a certain depth within the medium are analysed. These cases simulate topical application of photosensitiser and its intravenous injection and further accumulation in tumour, respectively.**

Keywords: *Monte Carlo simulation; fluorescence imaging, chlorin-based photosensitiser, photodynamic therapy.*

1. Introduction

Photodynamic therapy (PDT) is a modern therapeutic technique widely used for treatment of tumour and non-tumour pathologies. Its main mechanisms include cytotoxic effect, tumour vessels damage and immune reactions [1, 2]. PDT procedure starts with the administration of a photosensitiser (PS), which is selectively accumulated in tissues with increased microcirculatory activity, e.g. in tumours. The next step consists in PS activation with tissue irradiation at a certain wavelength of the visible range, which launches photochemical reactions resulting in the formation of cytotoxic products.

PDT efficacy depends on several factors, which include PS distribution within tissue, light propagation in tissues of different localisations and the absorbed light dose. The possibility of controlling these parameters allows the PDT efficacy to increase via individualisation of the PDT regime and correction of PS and light doses. Currently, PS and light doses are chosen empirically, and, for most cases, PS accumulation and photobleaching are not typically monitored.

A.V. Khilov, D.A. Kurakina, I.V. Turchin, M.Yu. Kirillin
Institute of Applied Physics, Russian Academy of Sciences, ul. Ulyanova 46, 603950 Nizhny Novgorod, Russia; e-mail: mkirillin@yandex.ru

Received 5 October 2018; revision received 9 November 2018
Kvantovaya Elektronika **49** (1) 63–69 (2019)
Translated by M.Yu. Kirillin

Since PS's are fluorescent markers, fluorescence imaging is commonly employed for PS accumulation monitoring. Selective PS accumulation in tumour tissues allows fluorescence imaging for *in vivo* tumour visualisation and for determination of borders between healthy and malignant tissues [3]. Chlorin-based PS's feature two peaks in their absorption spectra corresponding to 402 and 662 nm; hence, employment of a chlorin-based PS provides additional diagnostic opportunities. Since optical properties of biotissues, e.g. skin and mucosa, are different for the abovementioned wavelengths, the depth of light penetration in biotissues at these wavelengths also differs significantly. In this connection, fluorescence responses registered in course of dual-wavelength fluorescence imaging correspond to different probing depths, and their ratio provides the information about PS in-depth distribution [4]. In papers [4, 5] we suggested an approach to estimation of chlorin-based PS penetration depth based on fluorescence imaging with dual-wavelength excitation. PS penetration depth can be evaluated based on the measurements of the ratio of fluorescence responses corresponding to 662 and 402 nm excitation wavelengths. However, previously, we assumed PS distribution to be uniform in superficial tissue layer both for numerical simulations and model experiments with biotissue phantoms, which does not account for the features of real applications. PS diffuses into the tissue after topical application on skin or mucosa, which leads to nonuniform in-depth PS distribution [6]. The majority of models assume PS distribution to be uniform [7] after intravenous injection and further target delivery via blood flow; however, for that case the target region is located under the superficial layer without PS's. Thus, the previously suggested approach has to be adopted for nonuniform PS distribution after topical application and uniform PS distribution in target tissues after intravenous injection. Numerical simulations are the most efficient tool to study the formation of fluorescence signals with the possibility of controlling all the parameters, including different PS distributions.

Statistical Monte Carlo technique is widely used to study the propagation of light in biotissues. The Monte Carlo method is based on multiple calculations of random photon trajectories in a medium with specified optical properties and on further statistical data processing [8]. This method can be applied to simulate such an important parameter for PDT as the distribution of radiation in biological tissue of certain localisation [4]. The resulting maps of absorbed light dose distribution can be used for PDT planning to evaluate exposure areas for given irradiation regimes and local tissue optical properties. Various modifications of the Monte Carlo technique are employed to simulate and optimise optical imaging systems [9], including fluorescence approaches [10]. Numerical

simulations of fluorescence imaging allow the dependence of fluorescence response on simulation parameters to be determined. In paper [11], Monte Carlo simulations were used to study the effect of sample geometry on the registered fluorescence signal. In paper [12], Monte Carlo simulations were employed to study the dependence of fluorescence response on the irradiation configuration and optical properties of the medium. Numerical simulations of dual-wavelength fluorescence imaging for different models of PS administration (topical application and intravenous injection) allow studying the dependence of the fluorescence signals ratio on PS localisation.

The goal of this work is to develop an approach to estimation of chlorin-based PS localisation based on fluorescence signals ratio measurements in course of dual-wavelength fluorescence imaging with the excitation at the wavelengths of blue and red ranges, corresponding to chlorin e_6 absorption peaks. The study is based on Monte Carlo numerical simulations of fluorescence signals detected in fluorescence imaging.

2. Materials and methods

2.1. Monte Carlo simulations of fluorescence response

Numerical simulations of the PS fluorescence response were performed with the previously developed Matlab-based software for Monte Carlo simulations of light propagation in a layered medium [4, 13, 14]. Numerical simulations include two steps: At the first step, the volume distribution of the absorbed light dose at the excitation wavelength is calculated; the second step consists in calculation of fluorescence emission propagation from a distributed fluorescence source determined by PS volume distribution.

At the first step, the geometry of the medium (biotissue) and PS distribution are defined along with optical properties (absorption and scattering coefficients, anisotropy factor) of the medium and the PS, corresponding to the probe wavelength. For PS-containing layers, the absorption coefficient is calculated as the sum of medium and PS partial absorption coefficients. The map of the absorbed light dose distribution, which contains information about light dose absorbed in the unit volume of a medium, is calculated for the chosen source configuration and the excitation wavelength λ_{ex} along with the map of partial light dose distribution $A(x, y, z, \lambda_{ex})$ absorbed by the PS only. At the second step of the simulations, this partial absorbed light dose map is treated as a distributed fluorescence emission source, and the optical properties of the medium and the PS correspond to the emission wavelength. Emission of fluorescence photons is assumed to be isotropic in direction.

Thus, in Monte Carlo simulations the volume distribution of fluorescence emission $I_{fl}(x, y, z, \lambda_{ex}, \lambda_{em})$ at the emission wavelength λ_{em} from the PS distributed in the medium, is calculated as:

$$I_{fl}(x, y, z, \lambda_{ex}, \lambda_{em}) = \sum_{x', y', z'} A(x', y', z', \lambda_{ex}) I_{em}(x', y', z', x, y, z, \lambda_{em}), \quad (1)$$

where $I_{em}(x', y', z', x, y, z, \lambda_{em})$ is the volume distribution of the fluorescence emitted by a voxel with a unit weight and a centre at (x', y', z'). The fluorescence intensity distribution at the medium surface is a fluorescence image registered by a camera in course of fluorescence imaging.

2.2. Simulation parameters

For simulations, the excitation wavelengths λ_{ex} were chosen equal to 405 and 660 nm and the emission wavelength was chosen to be λ_{em} = 760 nm, which is determined by chlorin-based PS absorption and emission spectra (Fig. 1). However, the chosen values differ slightly from PS absorption and emission peaks and correspond to the wavelengths of sources applied for chlorin-based PS fluorescence imaging and the detection filter transmittance band allowing the excitation radiation to be cut off [15]. The simulations were performed for two cases: intravenous injection with the assumption of uniform PS distribution within the layer located at certain depth, and topical application corresponding to the exponential in-depth decay of PS concentration.

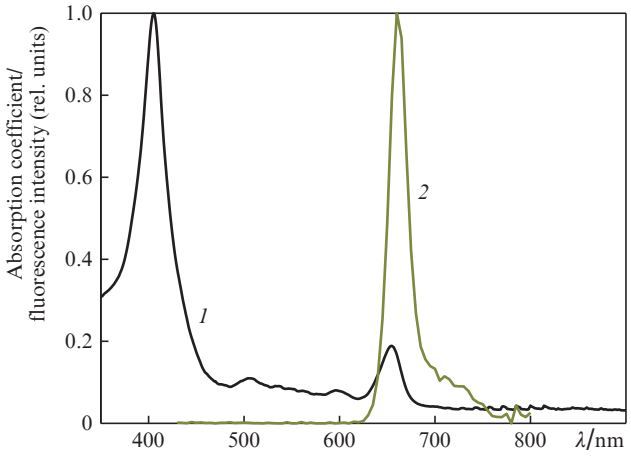

Figure 1. Chlorin-based PS (*1*) absorption and (*2*) fluorescence spectra.

In simulations of PS intravenous injection, the partial absorption map was calculated for the layer with uniform PS distribution. The layer thickness d and localisation depth z_0 varied from 0.25 to 3 mm (Fig. 2a). The PS volume concentration $C_{PS}(z)$ was assumed to be constant within the layer:

$$C_{PS}(z) = \text{const} = C_0. \quad (2)$$

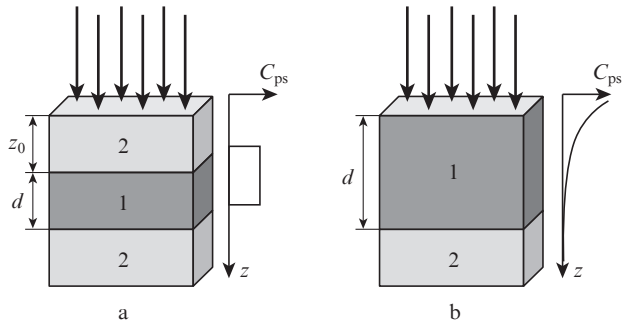

Figure 2. Geometry of numerical simulations and the PS concentration profile (a) for the fluorescent layer 1 in medium 2 and (b) for superficial fluorescent layer with exponential PS distribution.

The concentration C_0 was chosen equal to 0.5%, which corresponds to the estimation of a typical PS concentration in tissues [4].

In simulations of PS topical application, the partial absorption map was calculated for the upper layer which was additionally divided into layers with the discretisation of $\Delta z = 250$ μm and with constant volume concentration. The PS volume concentration $C_{PS}(z)$ was calculated in accordance with the exponential decay law

$$C_{PS}(z) = C_0 \exp(-\alpha z_i), \quad (3)$$

where z_i is the coordinate of the upper boundary of ith layer; $z \in [z_i, z_i+\Delta z]$; $C_0 = 0.5\%$; and $\alpha = 0.6$ mm^{-1} [16]. The discretisation value Δz was chosen to satisfy two conditions. On the one hand, it should exceed the photon free path in the medium to provide the local homogeneity of optical properties at the distance of photon free path for the Monte Carlo technique; on the other hand, it should ensure sufficient concentration changes within the entire fluorescent layer. The PS-containing layer thickness varied from 0.5 to 3 mm (Fig. 2b), and the concentration on the medium surface varied from $0.1C_0$ to C_0. For all the considered cases the medium dimensions were 10×10×6 mm; the number of photons was 10^7; and the distribution of probe irradiation at the medium surface was uniform (planar wave), which correspond to the distribution implemented in the experimental setup [15]. The fluorescence response was calculated by averaging fluorescence intensity $I_{fl}(x, y, z=0, \lambda_{ex}, \lambda_{em})$ over the medium surface for both excitation wavelengths λ_{ex}, and their ratio was calculated as

$$R_\lambda = \frac{\sum_{x,y} I_{fl}(x, y, z = 0, \lambda_{ex} = 660 \text{ nm}, \lambda_{em})}{\sum_{x,y} I_{fl}(x, y, z = 0, \lambda_{ex} = 405 \text{ nm}, \lambda_{em})}, \quad (4)$$

Table 1. Optical properties of medium and PS for Monte Carlo simulations.

Wavelength/nm	μ_a/mm^{-1}		μ_s/mm^{-1}	g	n
	Medium	PS ($C_0 = 0.5\%$)			
405	0.47	0.12	4.99	0.84	1.33
660	0.04	0.04	4.77	0.87	1.33
760	0.03	0.005	4.62	0.88	1.33

Note: μ_a is the absorption coefficient; μ_s is the scattering coefficient; g is the anisotropy factor; n is the refractive index.

similar to the value used in previous works on dual-wavelength fluorescence imaging [4, 13].

Medium optical properties were chosen equal to optical properties of the previously used biotissue phantom [5, 17]. Chosen optical properties for excitation and emission wavelengths are shown in Table 1. It should be mentioned that phantom optical properties slightly differ from those ones of skin [18]; however, as it was previously demonstrated in [5], variations of optical properties lead to quantitative, rather than qualitative, changes in the dynamics of R_λ. The refractive index was chosen equal to 1.33 assuming that the penetration of the PS solution increases biotissue hydration resulting in a refractive index close to that of water.

3. Results and discussion

3.1. Simulations of partial PS absorption maps

Monte Carlo simulations of the PS fluorescence response were performed for two cases: for a fluorescent layer within the tissue, which corresponds to PS accumulation in a tumour after intravenous injection, and for a fluorescent layer with exponential distribution, which corresponds to PS accumulation after topical application.

PS partial absorption maps for intravenous injection at both probe wavelengths for different depths and thicknesses

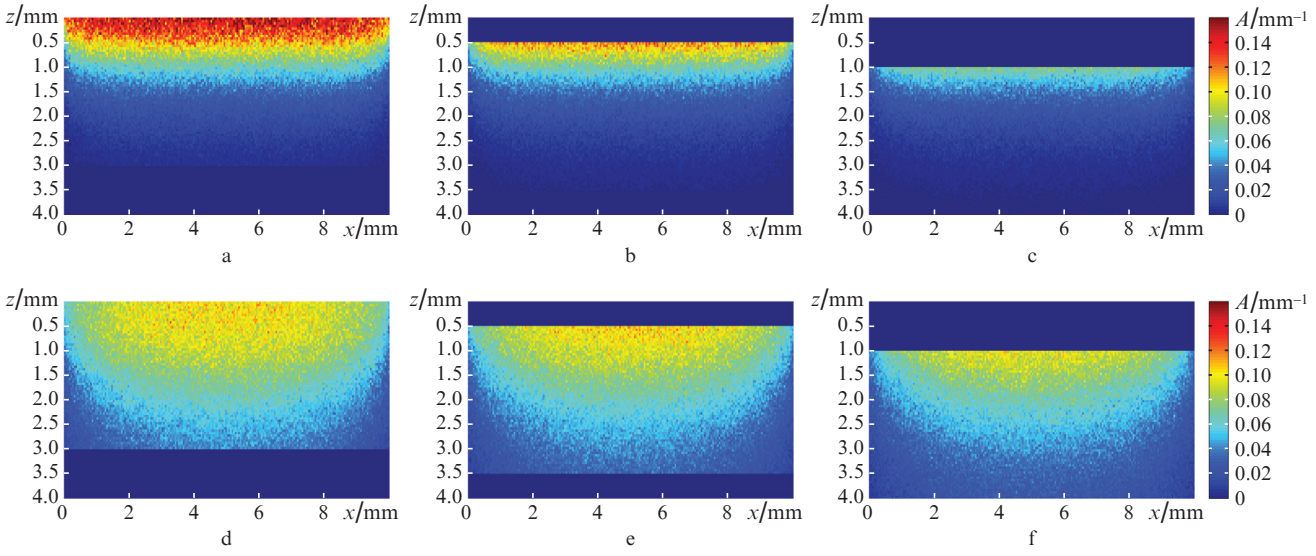

Figure 3. (Colour online) Maps of PS partial absorption $A(x, z, \lambda_{ex})$ in unit volume at excitation wavelengths of (a–c) 405 and (d–f) 660 nm for PS intravenous injection and 3-mm-thick fluorescent layer located at (a, d) medium surface, at (b, e) 0.5 mm depth and (c, f) at 1 mm depth. The maps are normalised to the number of launched photons per unit area.

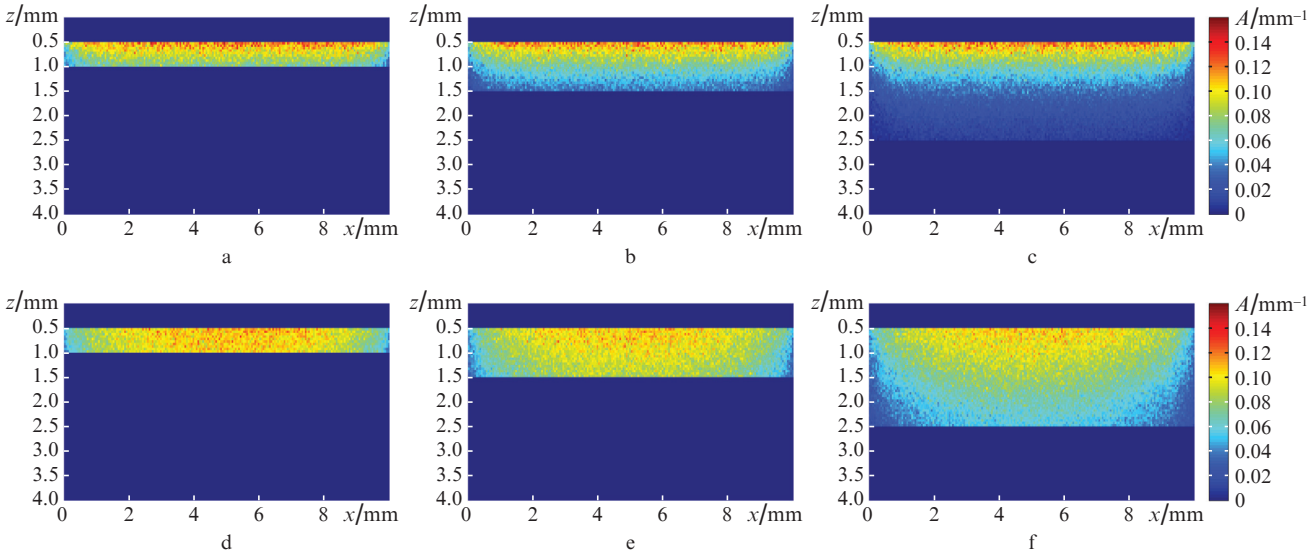

Figure 4. (Colour online) Maps of PS partial absorption $A(x, z, \lambda_{ex})$ in unit volume at excitation wavelengths of (a–c) 405 and (d–f) 660 nm for PS intravenous injection and fluorescent layer thickness of (a, d) 0.5 mm, (b, e) 1 mm and (c, f) 2 mm located at 0.5 mm depth within tissue. The maps are normalised to the number of launched photons per unit area.

of the PS-containing layer are shown in Figs 3 and 4, respectively.

As expected, the light dose absorbed by PS decreases with increasing fluorescent layer embedding depth, and the decrease is faster for 405 nm, which is associated with larger attenuation at this wavelength during propagation within the medium. It should be noted that the light dose absorbed by the PS in the upper layers at 405 nm significantly exceeds that at 660 nm, which is associated with larger PS absorption in the blue part of the spectrum.

Maps of PS partial absorption for the case of topical application are shown in Figs 5b and 5d. The maps for uni-

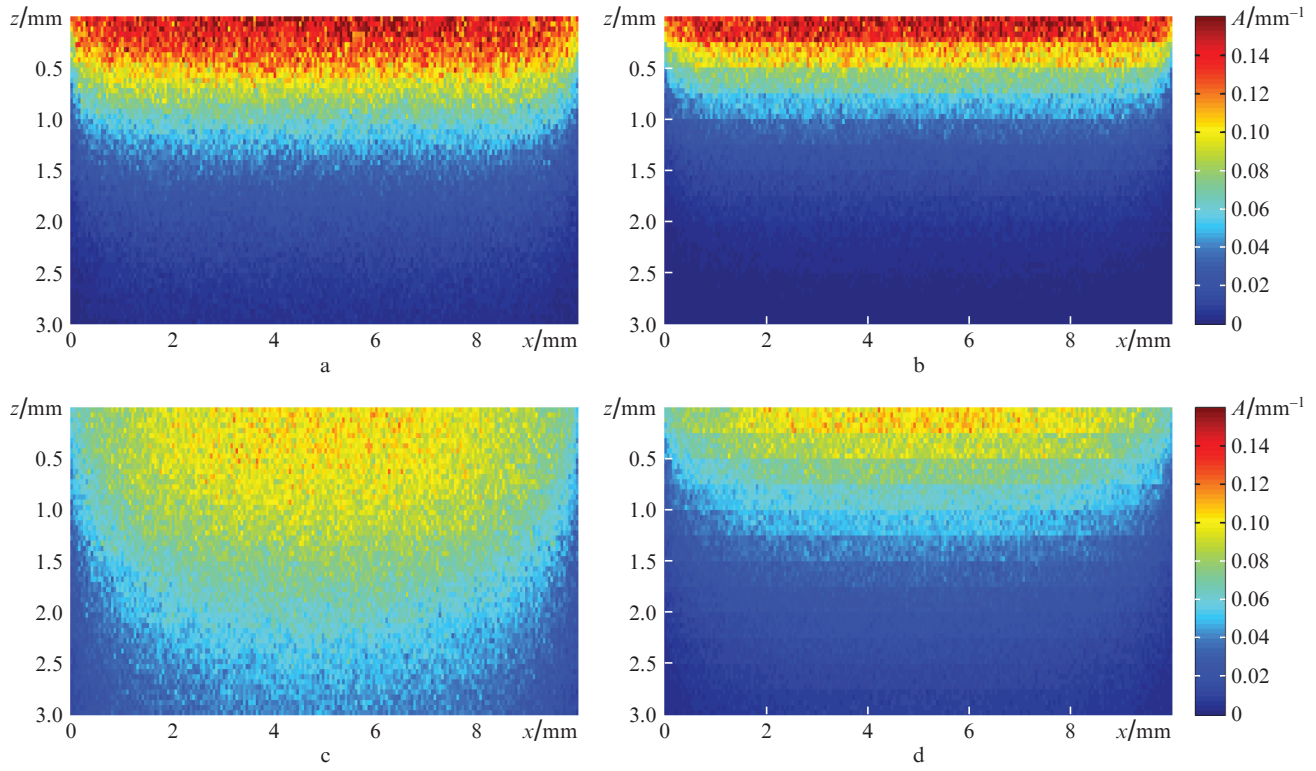

Figure 5. (Colour online) Maps of PS partial absorption $A(x, z, \lambda_{ex})$ in unit volume for PS topical application and (a, c) uniform and (b, d) exponential PS distribution at the excitation wavelengths of (a, b) 405 and (c, d) 660 nm. The maps are normalised to the number of launched photons per unit area.

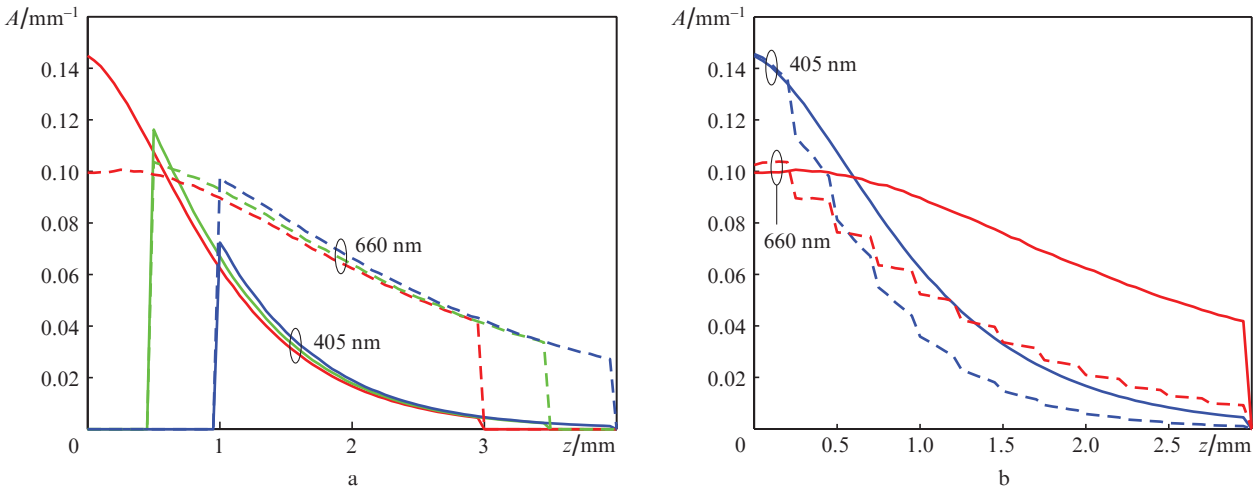

Figure 6. Central cross sections of the maps of PS partial absorption in unit volume for (a) 3 mm-thick fluorescent layer with uniform PS distribution at different depths and excitation wavelengths of 405 nm (solid lines) and 660 nm (dashed lines); (b) 3 mm-thick superficial fluorescent layer with uniform (solid lines) and exponential (dashed lines) PS distribution at excitation wavelengths of 405 nm and 660 nm. The map cross sections are normalised to the number of launched photons per unit area.

form PS distribution of the concentration C_0 are shown for comparison in Figs 5a and 5c.

As one can see from Fig. 5, the exponential in-depth decay of the PS concentration leads to absorbed light dose redistribution with an increase in superficial layers, and the effect is more significant for 660 nm, which is associated with the limited light penetration depth for blue light.

For the quantitative comparison of the effects the central cross sections of the PS partial absorption maps are plotted (Fig. 6). Figure 6a represents the cross sections for the PS uniformly distributed within a 3 mm-thick layer in the medium, and Fig. 6b corresponds to the case of PS uniformly and exponentially distributed within the superficial layer.

Thus, the major part of the light dose for excitation at 405 nm is absorbed in the upper layer, and for layer depths exceeding 2 mm the absorbed light dose and fluorescence response are relatively insignificant. However, as will be shown in Subsection 3.2, analysis of the ratio of the fluorescence signals allows both fluorescent layer thickness and its localisation depth to be evaluated. The curve decays for different fluorescent layer localisation depths are quite close for each excitation wavelength (Fig. 6a). However, the absorbed dose increases with increasing fluorescent layer localisation depth due to the lack of additional PS-associated light attenuation in the upper non-PS-containing layer. The waviness of the curves in Fig. 6b is related to the discreteness of PS concentration changes in the layer. Figures 5 and 6 show the necessity to account for the inhomogeneities in PS distribution in the upper layer in case of topical PS application.

3.2. Fluorescence signal ratio analysis

To study the feasibility of employment of the fluorescence signals ratio R_λ at the excitation wavelengths of 660 and

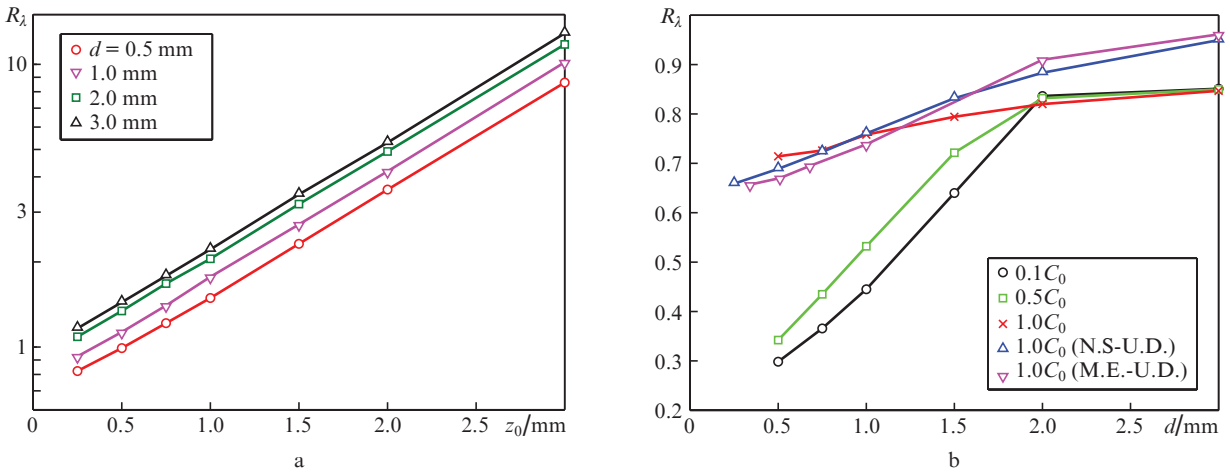

Figure 7. Dependences of the fluorescence signal ratio on (a) localisation depth of the fluorescent layer with thickness d in the case of intravenous injection and on (b) superficial layer thickness in the case of topical application with the comparison to numerical simulations data for uniform PS distribution in superficial layer (N.S-U.D.) and model experiment results for uniform PS distribution in superficial layer (M.E.-U.D.).

405 nm for evaluation of PS penetration depth, we calculated the dependences of this ratio on the embedding depth of a PS-containing layer and on the thickness of the layer for the cases of systemic injection and topical application, respectively. Figure 7a demonstrates the dependence of R_λ on the embedding depth of the PS-containing layer for the case of intravenous injection in logarithmic scale. The ratio of the fluorescence signals for a PS-containing layer with a constant thickness d increases with increasing its embedding depth that is explained by a fast decrease in the light dose absorbed by PS and stronger in-depth attenuation of probe radiation at the wavelength of 405 nm, while for the wavelength of 660 nm the effect is less pronounced. As one can see from Fig. 7a, the ratio R_λ of the fluorescence signals corresponding to two peaks in the chlorin-based PS absorption spectrum demonstrates an exponential law dependence on the layer embedding depth z_0, and the attenuation factor of this law does not depend on layer thickness. Hence, the R_λ value can be treated as a criterion for evaluation of the localisation depth z_0 of the fluorescent layer with known thickness d. A monotonous increase in R_λ with increasing layer thickness d additionally indicates that the R_λ value can be employed for evaluation of the PS-containing layer thickness d with the known localisation depth z_0, including $z_0 = 0$, i.e. for superficial localisations, which is in agreement with previously reported results [5].

The dependence of R_λ on the fluorescent layer thickness for the case of topical application, which accounts for an exponential in-depth drop of the PS concentration, at different PS concentrations is shown in Fig. 7b. For comparison, this figure also presents the results of numerical simulations and phantom experiment for the uniform PS distribution obtained in the framework of the previous study [5]. The dependences demonstrate a monotonous increase, and the rise in layer thickness d leads to the drop of the curve slope due to a decrease in the contribution of larger depths to the integral signal ratio. The rise of the R_λ value with the PS increase in the considered case originates from the fact that the absorption coefficients of the medium and the PS in the base concentration C_0 are comparable (see Table 1) for 660 nm, while for 405 nm the medium absorption coefficient is significantly larger than that of the PS. Hence, under excitation at 660 nm the increase in concentration gives a significant contribution to absorption of probe radiation, and fluorescence response rises stronger as compared with 405 nm, at which the high concentration does not provide such a significant increase in absorption. However, this effect leads to a decrease in penetration depth at 660 nm with increasing PS concentration, and the formation of the fluorescence response occurs in superficial layers, thereby decreasing the curve slope in the d range of 0.5–2 mm.

Comparative analysis of the ratio of fluorescence signals in the superficial layer for uniform and exponential PS distributions shows the necessity to account for inhomogeneity in PS in-depth distribution. Insignificant differences in the results for thin layers are associated with discreteness of the PS concentration changes in chosen numerical models.

4. Conclusions

Employing numerical simulations we have demonstrated the sensitivity of fluorescence responses to the PS localisation depth in biotissue in dual-wavelength fluorescence imaging. The suggested approach has been shown to provide the evaluation of fluorescent layer thickness in the case of known localisation depth and, vice versa, the evaluation of the PS-containing layer localisation depth, when its thickness is known, which is important when assessing PS accumulation in biotissue after intravenous injection. It also provides the evaluation of superficial PS-containing layer thickness with inhomogeneous PS distribution, which corresponds to PS penetration into biotissue after topical application.

The ratio of fluorescence signals, R_λ, at the wavelengths of 660 and 405 nm allows evaluating PS localisation after intravenous injection, and the dependence of this parameter on the PS-containing layer localisation depth demonstrates the exponential shape with the factor practically independent of the layer thickness. In the case of topical application, the sensitivity of the R_λ value to the PS penetration depth decreases with increasing depth, since the primary contribution to the detected signal in this case is given by superficial layers containing the maximal PS concentration.

The evaluation of PS localisation during its accumulation in tissues prior to PDT procedure can be of significant importance for the choice of irradiation wavelength and light dose delivered to tissue in course of the treatment, which will help to personalise the approach for a particular patient and improve PDT efficacy.

Acknowledgements. The work was supported by the Russian Science Foundation (Project No. 17-15-01264).

References

1. Celli J.P., Spring B.Q., Rizvi I., Evans C.L., Samkoe K.S., Verma S. *Chem. Rev*., **110** (5), 2795 (2010).
2. Allison R.R., Moghissi K. *Clin. Endosc*., **46** (1), 24 (2013).
3. He J., Yang L., Yi W., Fan W., Wen Y., Miao X., Xiong L. *Molecular Imaging*, **16**, 1 (2017).
4. Khilov A.V., Loginova D.A., Sergeeva E.A., Shakhova M.A., Meller E.A., Turchin I.V., Kirillin M.Yu. *Sovremennye Tekhnologii v Medicine*, **9** (4), 96 (2017).
5. Khilov A.V., Loginova D.A., Kirillin M.Yu., Turchin I.V. *Laser Phys. Lett*., **15**, 126202 (2018).
6. Svaasand L.O., Wyss P., Wyss M., Tadir Y., Tromberg B.J., Bern M.W. *Lasers Surg. Med*., **18**, 139 (1996).
7. Salas-García I., Fanjul-Vélez F., Arce-Diego J.L. *Intern. J. Photoenergy*, **2012**, 759205 (2012).
8. Wang L.V., Jacques S.L., Zheng L. *Comput. Meth. Progr. Biomed*., **47**, 131 (1995).
9. Genina E.A., Bashkatov A.N., Tuchin V.V., Altshuler G.B., Yaroslavsky I.V. *Quantum Electron*., **38** (6), 580 (2008) [*Kvantovaya Elektron*., **38** (6), 580 (2008)].
10. Periyasamy V., Pramanik M. *IEEE Rev. Biomed. Eng*., **10**, 122 (2017).
11. Welch A.J., Gardner C.M., Richards-Kortum R., Chan E., Criswell G., Pfefer J., Warren S. *Lasers Surg. Med*., **21**, 166 (1997).
12. Ong Y.H., Finlay J.C., Zhu T.C. *Proc. SPIE*, **10492**, 104920T (2018).
13. Shakhova M., Loginova D., Meller A., Sapunov D., Orlinskaya N., Shakhov A., Khilov A., Kirillin M. *J. Biomed. Opt*., **23** (9), 091412 (2018).
14. Kirillin M., Perekatova V., Turchin I., Subochev P. *Photoacoustics*, **8**, 59 (2017).
15. Kleshnin M.S., Fiks I.I., Plekhanov V.I., Gamayunov S.V., Turchin I.V. *Laser Phys. Lett*., **12**, 115602 (2015).
16. Lopez N., Mulet R., Rodríguez R. *J. Photochem. Photobiol. B*, **160**, 383 (2016).

17. Loginova D.A., Sergeeva E.A., Krainov A.D., Agrba P.D., Kirillin M.Yu. *Quantum Electron*., **46** (6), 528 (2016) [*Kvantovaya Elektron*., **46** (6), 528 (2016)].
18. Bashkatov A.N., Genina E.A., Kochubey V.I., Tuchin V.V. *J. Phys. D: Appl. Phys*., **38**, 2543 (2005).